Available online at www.sciencedirect.com

ScienceDirect

Combustion and Flame 153 (2008) 45–57

Combustion and Flame

www.elsevier.com/locate/combustflame

The ignition of methanol droplets in a laminar convective environment

R. Stauch *, U. Maas

Institut für Technische Thermodynamik, Universität Karlsruhe, Kaiserstrasse 12, D-76128 Karlsruhe, Germany

Received 14 November 2006; received in revised form 25 September 2007; accepted 17 December 2007

Available online 11 February 2008

Abstract

Numerical simulations of the ignition of methanol droplets in a laminar convective environment are performed using detailed reaction mechanisms and detailed transport models. The flow velocities of the forced convection ranges from 0.01 up to 5 m/s, whereas the ambient gas temperature is varied between 1300 and 1500 K. The ignition delay time of a single droplet is found to decrease with increasing velocity of the convective gas flow. This decrease is attributed to the steepening of the spatial gradients of the profiles of physical variables, such as species mass fractions or temperature. This steepening is originated by a stronger gas flow and leads to a speed-up of the physical transport processes. For the studied flow conditions, an acceleration of the gas flow on the order of the gravitational acceleration does not show a significant influence on the ignition delay time. A downstream movement of the local ignition point with increasing flow velocity is observed. For higher flow velocities, an ignition in the wake of the droplet followed by an upstream flame propagation is found. After ignition, the formation of an envelope flame is detected. The structure of this envelope flame is studied.

Keywords: Droplet; Detailed simulation; Ignition; Methanol

1. Introduction

For the understanding of spray combustion, a detailed knowledge of the processes associated with droplet ignition and combustion is required. Especially, a detailed understanding of the basic physical and chemical processes, such as vaporization, transport, and chemical kinetics, and their interaction is of interest. The ignition or combustion of single droplets in a quiescent atmosphere has been investigated in detail both experimentally and numerically for different fuels, e.g., methanol [1–3] and *n*-heptane [4–15], by a large number of research groups. However, in all technical applications, fuel droplets are exposed to a convective environment and to accelerating or decelerating forces. Thus, to achieve more reliable modeling of spray ignition and combustion, the influence of convective gas flow and relative acceleration of droplet and gas phase on the ignition and combustion of fuel droplets has to be investigated. A smaller number of studies deal with the influence of a convective air flow on the ignition or combustion behavior of fuel droplets [16–27], although in practical spray combustion devices, droplets are sub-

* Corresponding author.
E-mail address: stauch@itt.mach.uni-karlsruhe.de (R. Stauch).

0010-2180/$ – see front matter
doi:10.1016/j.combustflame.2007.12.001

jected to a convective environment. Tsai and Sterling [16] have studied the combustion of linear droplet arrays numerically by a quasi-steady approach with a one-step, finite-rate kinetic model. A quasi-steady approach with a one-step overall reaction, including a detailed multicomponent transport model, is also used by Pope and Gogos to study the influence of Lewis number and thermal diffusion effects on the modeling of the combustion behavior [23] as well as to investigate the extinction of n-heptane droplets due to forced convection [24]. The condensation of water during the combustion process and its influence on the evolution of the droplet diameter is studied experimentally in the case of freely falling methanol and ethanol droplets by Lee and Law [17]. Huang and Chen [18] have simulated the ignition of n-heptane droplets in a purely forced convective as well as in a mixed (forced and natural) convective environment using a one-step overall chemical reaction and a fixed Lewis and Prandtl number as well as a fixed value of the latent heat of n-heptane. Stapf et al. [20] have presented a two-stage model to simulate the combustion of Diesel sprays in internal combustion (I.C.) engines at high pressure. Transient numerical studies of surface tension effects and water absorption are performed by Raghavan et al. in the case of methanol droplet combustion under forced convection at different Reynolds numbers [25,26]. A significant dependence of the amount of absorbed water on the surface tension as well as on the Reynolds number was found. Furthermore, the influence of these effects on the extinction diameter of the droplets is studied. The influence of gravity on the flame of burning methanol droplets is also investigated numerically by Raghavan et al. [27]. Particularly, ignition delay times have been determined experimentally by Whang et al. [19] and Yang et al. [21] for n-heptane, n-hexadecane, and iso-octane. Qualitative numerical results for the ignition process of methanol droplets in air at high pressure and ignition delay times of droplets consisting of liquid oxygen in a hydrogen atmosphere have been presented by Aouina et al. [22]. Several studies deal with the phenomena of the influence of gravitational acceleration on the ignition behavior of droplets [7,12,28,29].

In this study the ignition of single methanol droplets in a convective air environment is investigated in detail. In the performed simulations, detailed models for the phase transition, the transport processes, and the chemical kinetics are applied. In the next section the mathematical model and its numerical solution are presented. In technical systems the droplets are exposed to a convective air flow. Thus, the dependence of the ignition delay time on the strength of the convective flow is studied. Because the ambient conditions of this flow are often changing with time, the influence of a relative acceleration of droplet and gas phase on these results is examined. To achieve information on the initiation and the process of ignition, the location and the mixture composition of the origin of ignition are observed. Methanol has been chosen as fuel because of the resulting feasible computational effort. Additionally, it should be mentioned that methanol is of interest as an alternative fuel [30,31].

2. Numerical model

To investigate the interaction of the physical and chemical processes, detailed numerical simulations are an efficient tool, because they make it possible to evaluate the contributions of chemical reactions, flow, and molecular transport. The presented model describes a spherical fuel droplet surrounded by an ambient gas phase. The droplet is exposed to a laminar convective gas flow. This system is analogous to a moving droplet in a gas environment with a relative velocity that is constant in time. In this approach the deceleration of the droplet due to friction forces and pressure drag is not taken into account, due to the steady inflow of the gas. Hence, it is assumed in this approach that the relative velocities of the droplet and the surrounding gas phase are constant in time. However, the viscous terms are included in the governing equations. Furthermore, the influence of the deceleration due to friction forces and pressure drag on the ignition process could be studied by a variation of the external deceleration, which is possible with the present model. Therefore, a long-range term of acceleration is added in the momentum equations. The boundary conditions are modified in a consistent way. The studied configuration is assumed to have rotational symmetry. The resulting computational domain, including the numerical grid, is shown in Fig. 1. The governing set of equations is given by the compressible Navier–Stokes equations for reacting flows [32–34].

Assuming a rotational symmetry, the results are independent of the azimuthal coordinate ϕ. (Note that the axis of symmetry, i.e., the z-axis, is parallel to the direction of the axisymmetric flow.) Hence, the number of independent variables is reduced to 3, namely the time t, the axial coordinate z, and the radial coordinate r:

$$\underbrace{f = f(x, y, z, t)}_{\text{3D}} \quad \rightarrow \quad \underbrace{f = f(r, z, t)}_{\text{2D}}. \tag{1}$$

The resulting equation system reads

$$\frac{\partial \rho}{\partial t} + \frac{1}{r}\frac{\partial}{\partial r}(\rho r v_r) + \frac{\partial}{\partial z}(\rho v_z) = 0, \tag{2}$$

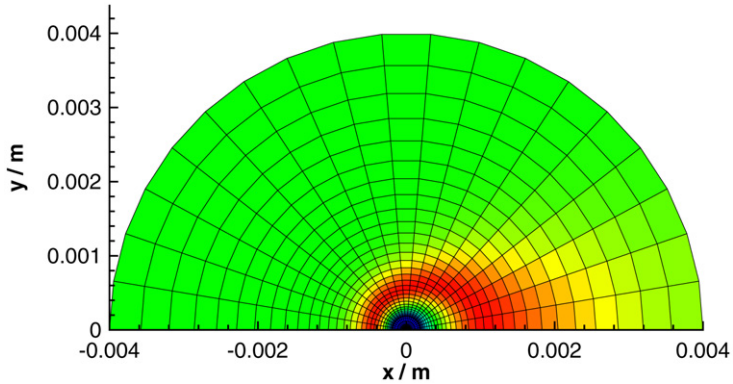

Fig. 1. Computational domain and numerical grid.

$$\frac{\partial \rho_i}{\partial t} + \frac{1}{r}\frac{\partial}{\partial r}(\rho_i r v_r) + \frac{\partial}{\partial z}(\rho_i v_z) + \frac{1}{r}\frac{\partial}{\partial r}\big(r(j_i)_r\big) + \frac{\partial}{\partial z}\big((j_i)_z\big) = M_i \dot{\omega}_i, \tag{3}$$

$$\frac{\partial(\rho v_r)}{\partial t} + \frac{1}{r}\frac{\partial}{\partial r}(\rho r v_r v_r) + \frac{\partial}{\partial z}(\rho v_r v_z) + \frac{\partial p}{\partial r} + \frac{1}{r}\frac{\partial}{\partial r}(r\Pi_{rr}) - \frac{\Pi_{\phi\phi}}{r} + \frac{\partial}{\partial z}(\Pi_{rz}) = \rho g_r, \tag{4}$$

$$\frac{\partial(\rho v_z)}{\partial t} + \frac{\partial}{\partial r}(\rho r v_r v_z) + \frac{\partial}{\partial z}(\rho v_z v_z) + \frac{\partial p}{\partial z} + \frac{1}{r}\frac{\partial}{\partial r}(r\Pi_{rz}) + \frac{\partial}{\partial z}(\Pi_{zz}) = \rho g_z, \tag{5}$$

$$\frac{\partial \rho u}{\partial t} + \frac{1}{r}\frac{\partial}{\partial r}(\rho u r v_r) + \frac{\partial}{\partial z}(\rho u v_z) + \frac{1}{r}\frac{\partial}{\partial r}\big(r(j_q)_r\big) + \frac{\partial}{\partial z}\big((j_q)_z\big) + p\left(\frac{1}{r}\frac{\partial}{\partial r}(r v_r) + \frac{\partial v_z}{\partial z}\right) + \Pi_{rr}\frac{\partial v_r}{\partial r} + \Pi_{\phi\phi}\frac{1}{r}\frac{v_r}{r} + \Pi_{zz}\frac{\partial v_z}{\partial z} + \Pi_{rz}\left(\frac{\partial v_r}{\partial z} + \frac{\partial v_z}{\partial r}\right) = 0. \tag{6}$$

The components of the stress tensor Π read [33]

$$\Pi_{rr} = -\mu\left(2\frac{\partial v_r}{\partial r} - \frac{2}{3}\left(\frac{1}{r}\frac{\partial}{\partial r}(r v_r) + \frac{\partial v_z}{\partial z}\right)\right), \tag{7}$$

$$\Pi_{\phi\phi} = -\mu\left(2\frac{v_r}{r} - \frac{2}{3}\left(\frac{1}{r}\frac{\partial}{\partial r}(r v_r) + \frac{\partial v_z}{\partial z}\right)\right), \tag{8}$$

$$\Pi_{zz} = -\mu\left(2\frac{\partial v_z}{z} - \frac{2}{3}\left(\frac{1}{r}\frac{\partial}{\partial r}(r v_r) + \frac{\partial v_z}{\partial z}\right)\right), \tag{9}$$

$$\Pi_{rz} = -\mu\left(\frac{\partial v_r}{\partial z} + \frac{\partial v_z}{\partial r}\right), \tag{10}$$

where ρ denotes the density, u the specific internal energy, ρ_i the partial densities, p the pressure, j_i the diffusion flux density of species i, ω_i the molar rate of formation of species i, M_i the molar mass of species i, and j_q the heat flux density. v_r and v_z are the velocity components in the radial and axial direction, respectively, and g_r and g_z the components of the (gravitational) acceleration.

The system of the Navier–Stokes equations has to be completed by an equation of state for both the gas and the liquid phase. The gas phase is assumed to be ideal. In the liquid phase the Hankinson–Brobst–Thomson technique is used to model the temperature dependence of the liquid density [35]. A vaporization model based on the assumption of local phase equilibrium accounts for the coupling of the liquid phase and the gas phase:

$$\phi_{\text{vap}} = \frac{-\sum_{j_{\text{vap}}} j_j^g}{\sum_{j_{\text{vap}}} \frac{p_j M_j}{p\bar{M}} - 1}, \tag{11}$$

$$0 = \rho^g \cdot v_n^g - \phi_{\text{vap}}, \tag{12}$$

$$0 = \phi_{\text{vap}}\big(w_i^g - \epsilon_i\big) + j_i^g, \tag{13}$$

$$0 = \sum_i \epsilon_i \cdot \phi_{\text{vap}} \cdot \Delta h_{\text{vap},i} + j_{q,c}^g - j_{q,c}^l. \tag{14}$$

ϕ_{vap} denotes the vaporization rate, w_i the species mass fraction, j_{vap} the index of the vaporizing species, p_j the partial pressure of species j, $\bar{M}$ the mean molar mass, v_n the velocity normal to the surface, $\epsilon_i = \dot{m}_i/\dot{m}$ the fraction of vaporizing mass, j_i^g the diffusion flux density of species i (gas phase), $\Delta h_{\text{vap},i}$ the enthalpy of vaporization of species i, and $j_{q,c}$ the conductive heat flux density. Due to its minor significance for the ignition process the influence of tangential stresses is neglected. Due to the low temperature and the small size of the droplet, the effects of radiation are neglected. The droplet is assumed to have a spherical shape and the regression rate of the droplet radius reads

$$\frac{dr_D}{dt} = -\frac{\phi_{\text{vap}}}{\bar{\rho}^l} - \frac{r_D}{2\bar{\rho}^l}\frac{d\bar{\rho}^l}{dt}, \tag{15}$$

where r_D denotes the droplet radius and $\bar{\rho}^l$ the mean liquid density of the droplet.

The chemical kinetics of methanol is modeled by a detailed reaction mechanism of Chevalier and Warnatz [34], consisting of 23 chemical species and 166 elementary reactions. The transport processes, are also modeled in detail. Fourier's law is used to determine the heat fluxes; the viscous terms are calculated by Newton's law of viscosity. The calculations of the viscosities and the thermal conductivities, as well as the diffusion coefficients, are based on kinetic theory [33,36,37]. For the determination of the diffusion coefficients the approximation of Curtiss and Hirschfelder [36,37] is used. The applied reaction mechanism, as well as the physical transport models, accounts for the correct pressure and temperature dependencies of the studied conditions. The Soret effect is taken into account, whereas the Dufour effect and mass diffusion due to a pressure gradient are neglected. Convection inside the droplet is neglected, whereas heat conduction in the liquid phase is taken into account. The physical properties of the liquid phase and of the phase transition are determined by the following correlations taken from Reid et al. [35]. The correlation of Latini et al. is used to calculate the heat conductivities; the approximation of Rowlinson and Bondi is applied to determine the specific heat capacities of the liquid phase. The vapor pressure is calculated following the Wagner equation, and the correlation of Riedel and Watson is used to calculate the enthalpy of vaporization. Hence, the presented model includes all occurring physical transport processes as well as chemical processes, except the effects mentioned above. The model is based on a former work of Aouina et al. [22], whereas the vaporization model has been improved. Furthermore, the temperature dependence of the liquid density has been implemented and the presented tool has been sped up to allow the execution of parametric studies.

The governing equations are solved in a fully coupled way by the method of lines using finite difference techniques. The equations are transformed into boundary-fitted curvilinear coordinates generated by TOMCAT [38]. The flux vector splitting upwind scheme of Steger and Warming [39,40] is applied to calculate the inviscid fluxes. The viscous fluxes are discretized using second-order central differences in chain rule conservation law form [41].

At the inflow, Dirichlet boundary conditions are used for the physical variables. At the outflow, the physical variables are assumed to have zero gradients. At the center line, standard symmetry boundary conditions are applied.

The time integration of the resulting differential–algebraic equation system is realized by the linearly implicit extrapolation method LIMEX [42]. Details on the numerical solution can be found in [22,41,43,44].

3. Results and discussion

The model presented above has been used to simulate the autoignition of single methanol droplets in a laminar convective environment. The surrounding gas phase consists of air in all cases. The ambient pressure has been set to $p = 7$ bar and the droplet radius to 200 μm, respectively. The ambient gas temperature varies between $T_g = 1300$ and 1500 K. In the following, aspects of the validation of the applied tool will be given. Subsequently, the influence of the convective flow and the relative acceleration of droplet and gas flow on the ignition delay time of methanol droplets is studied. Finally, the locations and the local states of the ignition points are investigated in more detail.

3.1. Validation of the tool

The presented tool has been constructed to be capable of simulating scenarios with spherical symmetry, too. This is done by a change of the boundary conditions. Thus, it is possible to compare results of simulations performed by the presented tool FLAME2D with results achieved by the one-dimensional tool, which has been presented in an earlier work [15]. The one-dimensional tool is based on the simulation tool INSFLA for simulating instationary ignition and combustion processes regarding inhomogeneities in one spatial coordinate [45,46]. INSFLA has been extended by implementing the detailed simulation of a liquid phase and the phase transition in one spatial coordinate. Therefore, it is possible to simulate the ignition and combustion behavior of single droplets under microgravity conditions [15].

In Fig. 2 the results of the simulation of a methanol droplet in quiescent surroundings, consisting of air at an ambient temperature of $T_g = 1400$ K and an ambient pressure of $p = 8$ bar are shown. Hence, a scenario with spherical symmetry is simulated for the validation of the presented tool. On the left side of Fig. 2, the spatial profiles of temperature of FLAME2D and INSFLA are compared. On the right side of Fig. 2, the spatial mass fraction profiles of methanol can be seen. The comparison is carried out at a time point before ignition (6.0 ms) and a time point after ignition (8.7 ms), when a flame around the droplet is established. As one can see, the profiles of FLAME2D and INSFLA almost coincide. Therefore, the positions of the flames are in good accord. The flame temperature of FLAME2D is about 80 K below the flame temperature of INSFLA. The ignition delay times are also compared. The simulation by FLAME2D provides an ignition delay time that is about 5% above the ignition time of INSFLA. These

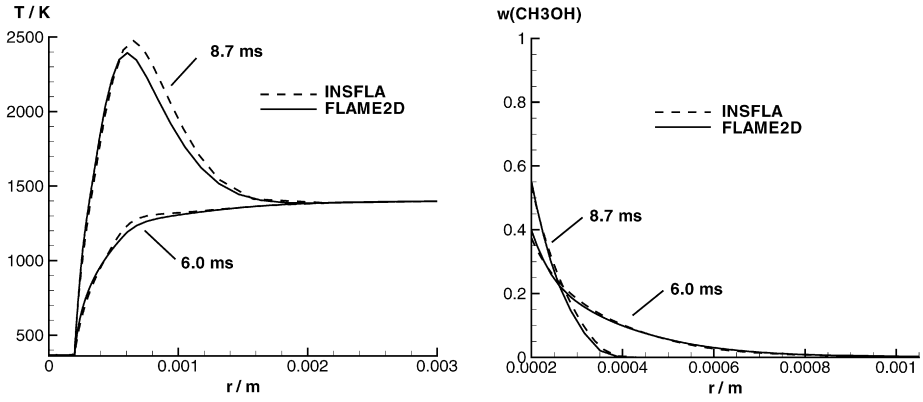

Fig. 2. Spatial profiles of temperature and methanol mass fraction of FLAME2D and INSFLA at two different times ($t_1 = 6.0$ ms, $t_2 = 8.7$ ms, $T_g = 1400$ K, $p = 8$ bar).

differences in the results originate in different numerical methods used in both tools. FLAME2D can be characterized by higher numerical diffusion due to the calculation of the convective fluxes, which is done by a first-order-accurate method. This problem is avoided in the case of the solution of the one-dimensional conservation equations (INSFLA) by a transformation into Lagrangian coordinates where the continuity equation is fulfilled identically [45]. Such a transformation would be very complicated for a system of two-dimensional conservation equations because a considerable distortion of the numerical grid can occur, which requires regularization [47]. The lower flame temperature in the two-dimensional case originates from the larger amount of numerical diffusion. Note, however, that the system of the governing equations is analytically equivalent. If the number of grid points of FLAME2D is increased by a factor of 2, the resulting flame temperature increases by a value of 50 K and thus it is only 30 K below the flame temperature of INSFLA. The ignition delay time in the case of the increased number of grid points still remains within the above mentioned uncertainty of 5%. Further performed calculations with an increased number of grid points have shown that the increase in the number of grid points leads to values even closer to the benchmark values. However, simulations are performed with the smaller number of grid points to achieve a feasible amount of computing time. Furthermore, the presented results are independent of the computational domain size.

These observations are confirmed by other test cases, which are not presented here. Finally, it can be stated that the results of the one- and two-dimensional simulations show good agreement. Thus, the presented tool FLAME2D can be used as a tool to investigate phenomena that can be reduced to a two-dimensional geometry.

3.2. Ignition delay times

In technical systems the combustion of droplets in a quiescent gas atmosphere under microgravity conditions does not occur because there is at least gravitational acceleration. Furthermore, the fuel droplet is usually exposed to an ambient gas flow. Concerning the autoignition of a fuel droplet, it is of great interest how the ignition process is influenced by the gas flow. It can be stated that due to the fact that the system has no spherical symmetry any more, the ignition process changes significantly. In contrast to the microgravity case, the flame front does not have a spherical shape anymore [18,19,22]. The described changes in the studied system can also affect the ignition delay time. Thus, the influence of a laminar convective environment on the ignition delay time is investigated in this section.

In Fig. 3 the dependence of the ignition delay time on the convective flow in terms of the (droplet) Reynolds number is shown. The flow velocity has been varied from 0.1 to 10 m/s at three different gas temperatures. Following the definition of the (droplet) Reynolds number,

$$\mathrm{Re} = \frac{v_\infty \cdot d_D}{\nu_\infty}, \tag{16}$$

where v_∞ and ν_∞ denote the velocity and the kinematic viscosity of the ambient air and d_D the droplet diameter, these flow velocities correspond to (droplet) Reynolds numbers in the range from 0.5 to 80.

A significant decrease of the ignition delay time with increasing flow velocity can be observed. As one can see a variation of the flow velocity by an order of magnitude has a comparable effect on the ignition delay time to a variation of the gas temperature by ± 100 K. Because of the logarithmic scaling of both axes and the shape of the underlying curve of the data, a dependence of the ignition delay time

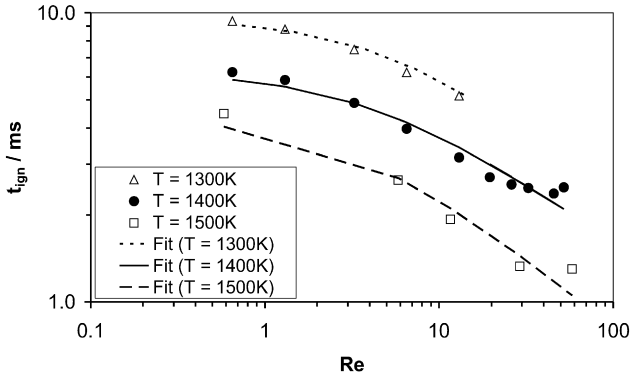

Fig. 3. Dependence of the ignition delay time on the (droplet) Reynolds number of the convective gas flow ($p = 7$ bar, $r_D(0) = 200$ μm).

Table 1
The fit parameters a, b of the dependence of the ignition delay time on the (droplet) Reynolds number for three different gas temperatures

T_g	a	b
1300 K	0.17	−0.49
1400 K	0.25	−0.41
1500 K	0.29	−0.49

on the (droplet) Reynolds number similar to a potential law is suggested. The obtained results are represented by the following simple curves describing the dependence of the ignition delay time on the (droplet) Reynolds number:

$$t_{\text{ign}}(\text{Re}) = t_{\text{ign}}(\text{Re} = 0) \cdot (1 + a \cdot \text{Re})^{b}. \tag{17}$$

$t_{\text{ign}}(\text{Re})$ denotes the ignition delay time depending on the (droplet) Reynolds number Re, $t_{\text{ign}}(\text{Re} = 0)$ is the ignition delay time if no gas flow is present, and a, b are fit parameters, which are presented in Table 1. The resulting fitted curves for the three different temperatures are shown in Fig. 3, too. It can be stated that for the investigated circumstances, the fitted curves show reasonable agreement with the data of the detailed simulation. At high values of the Reynolds number (>40), the curve fit does not represent the data well. This can be explained by the fact that the strain rate of the system increases and the ignition process is delayed. At higher velocities, no ignition at all, or at least no ignition within the computational domain, occurs. The obtained fit parameters differ only slightly, as can be seen in Table 1. Due to the fact that only the ignition delay time of the droplet in the quiescent gas phase and two additional fit parameters are necessary to fit the data points, a general trend in the observed data seems to exist. Furthermore, this trend bears a certain resemblance to the correlation of Ranz and Marshall, which describes the influence of an inertial gas flow on the Nusselt and the Sherwood number [48,49],

$$\text{Nu}, \text{Sh} \propto (1 + c \cdot \text{Re}^{0.5}), \tag{18}$$

where c describes a constant depending on the Prandtl and the Schmidt number, respectively. It has to be noted that if the ignition process is rate-limited by transport processes in the boundary layer, the typical timescale of the ignition process t_{ign} would be proportional to the typical timescale of these transport processes τ_{trans}, and therefore to the inverse of Nu and Sh, respectively. In this context, the similarity of the exponents b in Table 1 to -0.5 is noticeable. Furthermore, because a higher value of a means a stronger dependence of the ignition delay time on the Reynolds number, the influence of the gas flow increases for increasing ambient temperature. It is supposed that this behavior is originated by the fact that transport processes become more and more rate-limiting due to the increasing Damköhler number with increasing ambient temperature. The Damköhler number is defined as the ratio of transport timescale τ_{trans} and chemical timescale τ_{chem},

$$\text{Da} = \frac{\tau_{\text{trans}}}{\tau_{\text{chem}}}, \tag{19}$$

and is increasing because of the exponential decrease of the characteristic chemical timescale. The reasons that lead to decreasing ignition delay times with increasing gas flow velocity will be investigated in more detail in the next section.

In technical systems, fuel droplets are accelerated and decelerated compared to the gas phase. Therefore, we study the influence of relative acceleration between droplet and gas phase on the ignition delay time for a range of different initial relative velocities. The direction of the acceleration and of the gas flow are set parallel. The implementation of an acceleration is done by adding the long-range term of acceleration in the momentum equation. The boundary conditions

are modified in a consistent way. The magnitude of the relative acceleration is set to the value of the gravitational acceleration $a = g = 9.81\ \mathrm{m/s^2}$. Following the definition of the Froude number [33],

$$\mathrm{Fr} = \frac{v_0^2}{d_D \cdot g}, \tag{20}$$

where v_0 denotes the initial gas flow velocity, the Froude number ranges from 0.025 to 250 for the studied velocities. This allows conclusions about the influence of acceleration on the ignition process of droplets. Fig. 4 shows the simulated setup, including the parallel directions of gas flow and acceleration a. In Fig. 5 the dependence of the ignition delay time on the initial gas flow velocity v_0 with and without the presence of relative acceleration is compared. It can be seen that occurrence of the acceleration does not change the ignition delay time significantly. Compared to the influence of the initial velocity of the gas flow, v_0, the influence of gravitational acceleration can be neglected. This result can certainly be expanded on the influence of any acceleration of the order of magnitude of the studied acceleration or less. A change of the direction of the acceleration relative to the initial velocity does not increase the influence more than in the studied case, because the temporal change of the velocity is greatest in the studied case, due to the parallelism of the two vectors. Cases of an initial velocity higher than 1 m/s have not been studied, because the relative change of velocity would be even smaller than in the studied cases. One reason for this minor influence is the fact that the change of the relative velocity within the duration of the ignition process (7 ms) is at most 0.07 m/s. Therefore, the velocity of the gas phase relative to the droplet does not change considerably for higher initial velocities within the duration of the ignition process. For lower initial velocities, where a considerable increase of the relative velocity during the ignition process is present, the dependence of the ignition delay time on the gas flow velocity is not that strong and so the acceleration does not have a significant influence on the ignition delay time. The identification of a minor influence of gravity on the ignition delay times of droplets corresponds with the experimental results of Faeth and Olson [28], Tanabe et al. [7], and Schnaubelt et al. [12] for other fuels (n-heptane, n-hexadecane, benzene).

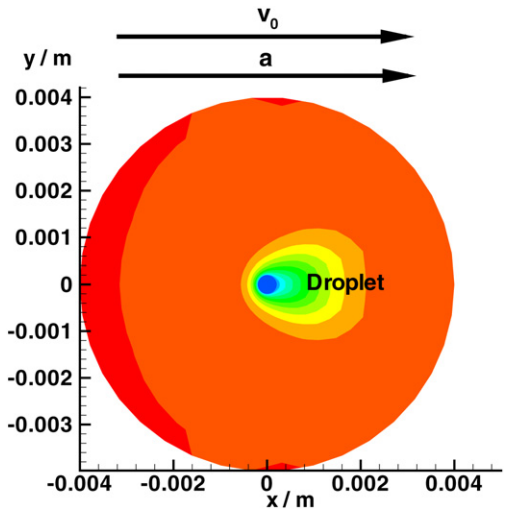

Fig. 4. Setup of simulation including gravitational acceleration.

3.3. Ignition locations and ignition states

The influence of the laminar convective flow on the ignition delay time raises the question about the reason for the speedup of the ignition process. Therefore, the spatial profiles of the temperature and some species upstream of the droplet are investigated in more detail. Fig. 6 shows the profiles of the temper-

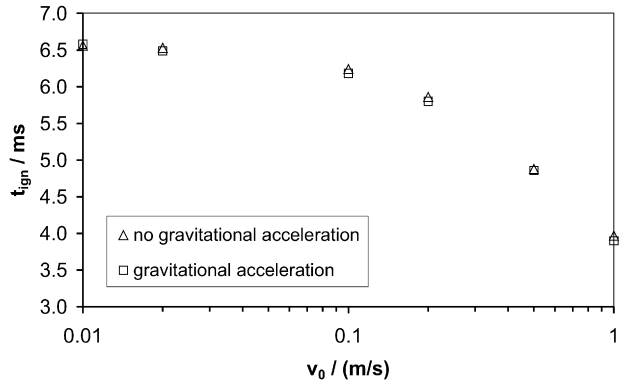

Fig. 5. Dependence of the ignition delay time on the convective velocity of the gas flow (with and without the influence of acceleration) ($T_g = 1400$ K, $p = 7$ bar, $r_D(0) = 200$ µm).

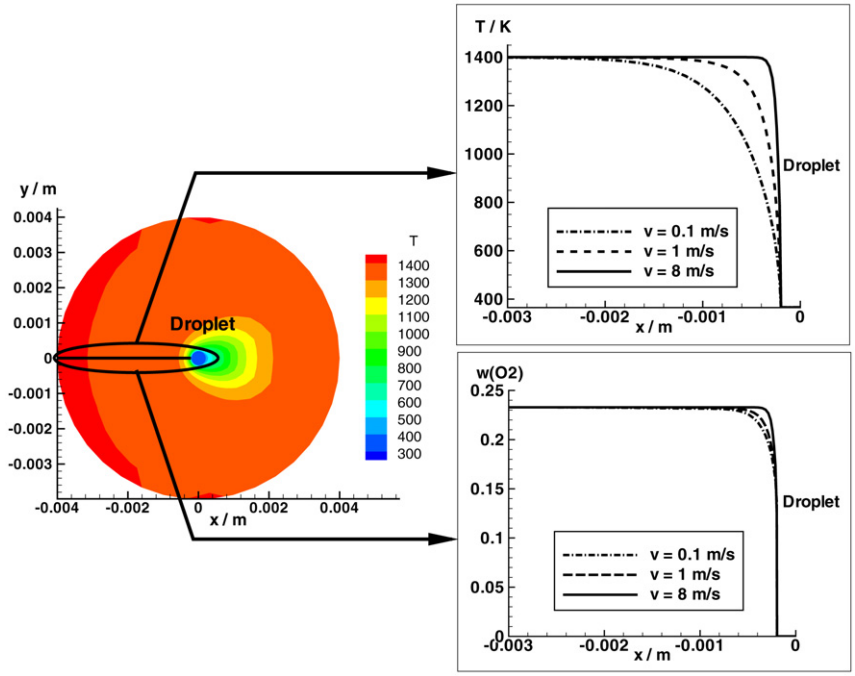

Fig. 6. Profiles of temperature and oxygen mass fraction along the upstream x-axis (indicated line) ($T_g = 1400$ K, $p = 7$ bar, $r_D(0) = 200$ μm, $t = 2$ ms).

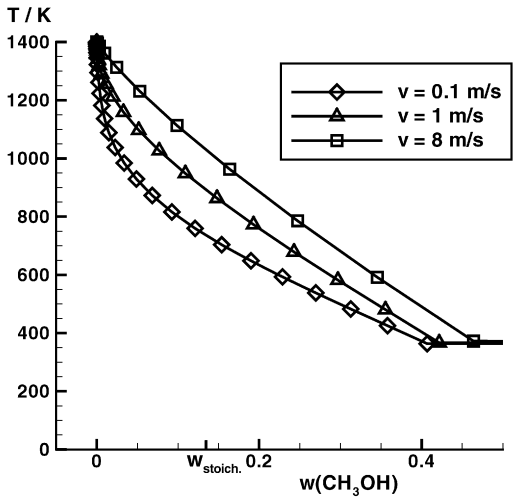

Fig. 7. Projection of the state space onto the temperature/methanol mass fraction plane for the upstream x-axis ($T_g = 1400$ K, $p = 7$ bar, $r_D(0) = 200$ μm, $t = 2$ ms).

ature and the mass fraction of molecular oxygen for three different gas velocities along the indicated line at a time of 2 ms. It can be seen, that a higher velocity leads to profiles, which are more steepened compared to the profiles of lower velocities. Stronger convection results in steeper gradients. These steeper gradients lead to a speedup of diffusive processes such as mass diffusion and heat conduction. To investigate the influence of the accelerated diffusion on the ignition process, the profiles mentioned above are shown as local states in the state space in Fig. 7. On the x-axis the species mass fraction of methanol is plotted. On the y-axis the temperature of the local state is plotted. For a particular species mass fraction of methanol, the local temperature is higher, with a higher gas flow velocity. This higher temperature leads to an acceleration of the local chemical kinetics, which results in a speedup of the ignition process. Besides that, the speedup of the diffusive processes leads to an increase of the vaporization rate of the droplet because the vaporization process of droplets is limited by the diffusive processes, such as heat conduction and mass diffusion [34,49–51]. Due to the increased vaporization rate, the necessary fuel vapor for ignition is more rapidly available. This is why a stronger convective flow leads to acceleration of the ignition process, as is shown in Fig. 3. It has to be noted that a further increase of the gas flow velocity leads to an absence of ignition due to the sweeping away of the fuel vapor and the preventing of the formation of a reactive mixture. This effect is even more likely in the case of lower ambient gas temperatures. These observations lead to the conclusion that physical transport processes, such as heat conduction, mass diffusion, and vaporization, are rate-limiting with respect to the ignition process. This is consistent with

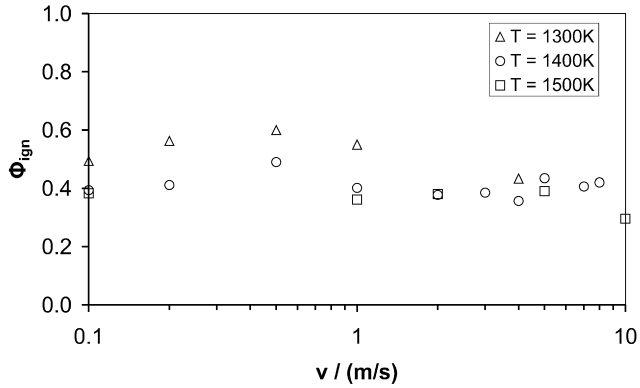

Fig. 8. Dependence of the local equivalence ratio of the ignition point on the convective velocity of gas flow ($T_g = 1400$ K, $p = 7$ bar, $r_D(0) = 200$ μm).

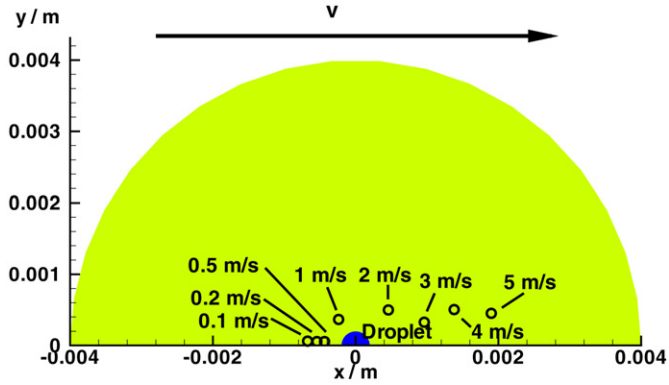

Fig. 9. Dependence of the location of the ignition point on the convective velocity of gas flow ($T_g = 1400$ K, $p = 7$ bar, $r_D(0) = 200$ μm).

the fact that the Damköhler number is high at the studied gas temperatures, due to the small chemical timescale. This conclusion corresponds with previous findings for a comparable temperature range for the case of *n*-heptane [15].

Another important aspect with regard to droplet ignition is the local equivalence ratio at the ignition point. For example, it is possible that ignition of the fuel occurs under locally lean conditions, although the overall equivalence ratio is fuel-rich. Therefore, the influence of the gas flow velocity on the local equivalence ratio of the ignition point is studied. Fig. 8 shows the dependence of the local equivalence ratio of the ignition point on the gas flow velocity for three ambient gas temperatures. The equivalence ratio remains almost constant over a range of two orders of magnitude of the velocity for all three temperatures. All observed states show an equivalence ratio at the ignition location between 0.3 and 0.6, which means that the ignition occurs under lean conditions. This behavior bears a strong resemblance to previous results on the ignition of *n*-heptane droplets in a quiescent gas environment [15].

Even if the local equivalence ratio of ignition is not affected very much by the velocity of the gas flow, the ignition process is modified significantly by the varied gas flow velocity. The local point of ignition moves gradually from the upstream region of the droplet at lower velocities to the wake of the droplet at higher flow velocities. This is illustrated in Fig. 9, in which the different points of ignition depending on the gas flow velocity are shown. The points are indicated by the associated velocity of the gas flow. In all investigated cases up to a flow velocity of 5 m/s, the formation of an envelope flame can be observed after ignition. These findings show resemblance to the observations of Whang et al. [19], who observed the formation of an envelope flame in all studied cases of *n*-heptane and *n*-hexadecane droplets. The formation of the envelope flame is associated with an upstream flame propagation if the ignition occurs in the wake of the droplet. The flame propagating upstream is observed in our numerical studies for the cases of a

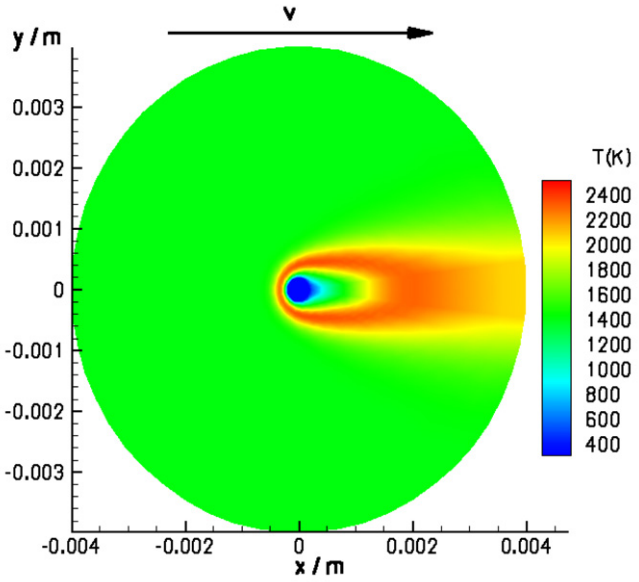

Fig. 10. Shape of the envelope flame (temperature distribution; $v_\infty = 4$ m/s, $T_g = 1400$ K, $p = 7$ bar, $r_D(0) = 200$ μm, $t = 9$ ms).

Table 2
Flame propagation speeds for different droplet velocities ($T_g = 1400$ K, $p = 7$ bar, $r_D(0) = 200$ μm)

v_∞	v_{flame}
3 m/s	6.01 m/s
4 m/s	5.53 m/s
5 m/s	6.32 m/s

flow velocity between 3 and 5 m/s. Table 2 shows the three determined speeds of the flame propagating upstream. The flame propagation speed may not be identified with a flame velocity. In fact, it denotes the speed at which the reaction zone moves upstream after ignition of the fuel in the wake of the droplet. The flame propagation speeds are achieved by adding the free-stream velocities to the observed velocities. This guarantees comparability of cases with different free-stream flow velocities and the results of Whang et al. [19]. The values of the propagation speeds are comparable with the laminar flame velocity of about 5.5 m/s of a stoichiometric mixture of methanol and air at a pressure of 7 bar and at an unburned gas temperature of 1000 K. The laminar flame velocity has been calculated by numerical simulation including detailed transport models and the detailed reaction mechanism of Chevalier and Warnatz [34,45,46,52]. The propagation speeds are also in the same order of magnitude like the flame propagation speeds of Whang et al. [19] which are in the range from 4 up to 7.5 m/s. A more detailed comparison of the propagation speeds is difficult because the speeds have been obtained with different fuels and at different temperatures. These two parameters are influencing the propagation speed, as Whang et al. have pointed out. They observed an increase of the propagation speed with increasing gas temperature. In contrast, a tendency of the propagation speed with varying flow velocity at a fixed gas temperature cannot be observed in the studied cases. Furthermore, Raghavan et al. have simulated the auto-ignition process of a methanol droplet numerically [25]. Their results also exhibit an upstream flame propagation, but the effect is not studied in detail.

Further studies with lower gas flow velocities and at lower gas temperatures could confirm the quantity of this flame propagation speed. These studies involve a remarkable increase of computing time because of the increase of the ignition delay time with lower flow velocities and lower gas temperatures.

3.4. Properties of the envelope flame

Some properties of the envelope flame are studied, so that a more detailed characterization of the phenomenon of the combustion of a single fuel droplet is possible. Fig. 10 shows the droplet and the envelope flame for a flow velocity of 4 m/s. The spatial temperature distribution is presented at a considerable time after ignition and upstream flame propagation (note that the ignition has occurred at a time of about 3 ms). The influence of the forced convection on the shape of the flame can be seen clearly. To characterize the observed envelope flame the dependence of

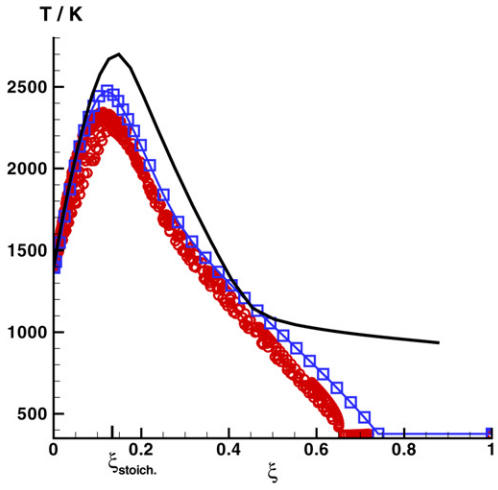

Fig. 11. Dependence of the local temperature on the mixture fraction. ○: States of the envelope flame, □: spherical flame without a convective air flow, ∧: line of adiabatic equilibrium (stoichiometric mixture fraction: $\xi_{\text{stoich.}} = 0.1345$, $v_\infty = 4$ m/s, $T_g = 1400$ K, $p = 7$ bar, $r_D(0) = 200$ μm, $t = 9$ ms).

the temperature on the mixture fraction ξ is investigated. This dependence is illustrated in Fig. 11. The stoichiometric mixture fraction of the methanol/air mixture is $\xi_{\text{stoich.}} = 0.1345$. The circles represent the observed mixture fractions of the envelope flame at a time of $t = 9$ ms. The line with squares depicts the dependence of the temperature on the mixture fraction in the case of a spherical flame burning around a droplet in a quiescent gas atmosphere. The line illustrates the states of adiabatic equilibrium calculated by the chemical equilibrium program GASEQ [53]. Note that the equilibrium for $\xi_{\text{stoich.}} > 0.4$ does not represent an approximation to the simulation data, because the fuel methanol is decomposed to CH_4, CO, CO_2, H_2, and H_2O in the equilibrium. The deviation of the droplet flame data from the adiabatic equilibrium becomes very large for $\xi_{\text{stoich.}} > 0.4$. This is due to both the physical transport processes and the boundary conditions at the droplet surface, which are described below. In the case of the investigated droplet combustion, no states are observed for mixture fractions larger than 0.7. This is caused by the fact that the droplet temperature does not reach the boiling temperature of the fuel. In fact, the steady-state temperature or wet-bulb temperature of the droplet is below the boiling temperature [54–56]. Accordingly, the mass fraction of the fuel and therefore the mixture fraction in the gas phase can only reach values according to the vapor pressure at the wet-bulb temperature of the droplet. As can be seen, the temperature at a certain mixture fraction is reduced in the case of droplet combustion compared to the adiabatic equilibrium. This is due to the heat conduction. The influence of the heat conduction is greatest at the flame, i.e., at the stoichiometric mixture fraction, and at the very rich states ($\xi > \xi_{\text{stoich.}}$) that are located spatially next to the droplet. In the case of adiabatic equilibrium, the temperature is considerably higher because the fuel methanol is decomposed. In the cases of the droplet flames, the boundary condition at the droplet surface is given by a methanol/air mixture and the methanol cannot be decomposed. Additionally, due to the lower temperature of the droplet compared to the ambient air and the proximity of the flame to the droplet the local temperature gradient is considerably steep. This leads to a major amount of heat, which dissipates. For lean states ($\xi < \xi_{\text{stoich.}}$), a minor reduction of the temperature is obtained. This is caused by both the higher temperature of the ambient air compared to the droplet and the absence of a near boundary with a fixed temperature like the droplet surface. Furthermore, the temperatures at a certain mixture fraction ξ are lower in the case of the envelope flame compared to the spherical flame due to the inertial gas flow. This finding can be explained by the occurring increased local strain rates. As shown in Section 3.3, this leads to a steepening of the spatial temperature and species profiles and therefore to a speedup of the heat conduction.

Nevertheless, the states in the state space, illustrated in Fig. 11, of both the spherical and the envelope flame are located close to a one-dimensional manifold. This allows a description of both flames by a reduced number of variables. Furthermore, the results lead to the conclusion that the envelope flame can be approximated by a diffusion flame with fast chemical kinetics compared to the physical transport processes. The finding of other studies, that the physical transport processes are rate-limiting at such gas temperatures [15], is confirmed. This finding also allows the assumption that the behavior of a burning methanol droplet can be described by simpler chemical kinetics. However, these conclusions do not hold during the process of ignition, where the obtained mixture fractions do not bear such a resemblance to the ideal case of complete conversion.

4. Conclusions

The autoignition process of methanol droplets in a convective environment is investigated numerically. The simulations are performed by the tool FLAME2D by solving the governing equations of the gas and the liquid phase fully coupled including a detailed vaporization model, a detailed transport model, and a detailed reaction mechanism.

The influence of a gas flow on the ignition process is investigated. The ignition delay time decreases with an increasing velocity of the gas flow for three different ambient gas temperatures. The obtained results of the decreasing ignition delay times can be represented by a potential law depending on two fit parameters. These fit parameters show similar values for all three investigated gas phase temperatures, which indicates a general influence of the inertial gas velocity or the Reynolds number on the ignition delay time.

To investigate this influence in detail the shift of spatial profiles due to a convective velocity is analyzed. The stronger convection results in steeper gradients in the upstream region of the droplet. This leads to a higher local temperature at a given species composition or a local equivalence ratio closer to stoichiometry at a given temperature, respectively. This results in an acceleration of the chemical kinetics, which complies with a speedup of the ignition process.

The local equivalence ratio is analyzed and the occurrence of ignition at locally lean mixtures is found. This behavior holds for all studied cases. The equivalence ratios are between 0.3 and 0.6 which points out the ignition under lean conditions. This behavior is almost not affected by the varying gas flow velocity, and even more, but only a little, by the ambient gas temperature.

However, the ignition process as a whole is quite remarkably affected by a modified gas flow velocity. With an increasing flow velocity the location of ignition is moving from upstream of the droplet around the droplet to the wake of the droplet. Up to a flow velocity of 5 m/s the formation of an envelope flame is detected. For flow velocities from 3 to 5 m/s ignition occurs downstream of the droplet and upstream flame propagation can be observed. The obtained propagation speeds for methanol are in the range from 5 to 7 m/s, which is in agreement with the findings of Whang et al. for *n*-heptane and *n*-hexadecane [19]. A dependence of the propagation speed on the flow velocity cannot be observed.

Furthermore, properties of the envelope flame are studied. The observed dependences of the temperature on the mixture fraction lead to the conclusion that the envelope flame corresponds to a diffusion flame type with fast chemical kinetics, after the ignition process has completed and a quasi-steady burning behavior has occurred. Nevertheless, the influence of the dissipation of heat by heat conduction is clearly observable.

To investigate the upstream flame propagation and the characteristics of the envelope flame in more detail, simulations have to be performed with lower gas flow velocities at lower ambient temperatures, where the chemical kinetics play a major role for the time scales of the ignition and combustion process of a droplet. This involves a considerable increase of computing time. Therefore, the further improvement of the numerical solution of the governing equations with respect to a speedup of the solution procedure is a subject of future work.

Acknowledgments

The authors thank the DFG for financial support in the frame of SFB 606. The simulations were performed on the national supercomputer NEC SX-8 at the High Performance Computing Center Stuttgart (HLRS) under Grant flame2D/12792.

References

[1] S. Cho, M. Choi, F. Dryer, Proc. Combust. Inst. 23 (1990) 1611–1617.
[2] S. Cho, R. Yetter, F. Dryer, J. Comput. Phys. 102 (1992) 160–179.
[3] P. Stapf, Ph.D. thesis, Universität Stuttgart, 1992.
[4] H. Hara, S. Kumagai, Proc. Combust. Inst. 23 (1990) 1605–1610.
[5] M. Takei, T. Tsukamoto, T. Niioka, Combust. Flame 93 (1993) 149–156.
[6] R. Nakanishi, H. Kobayashi, S. Kato, T. Niioka, Proc. Combust. Inst. 25 (1994) 447–453.
[7] M. Tanabe, M. Kono, J. Sato, J. Koenig, C. Eigenbrod, F. Dinkelacker, H. Rath, Combust. Sci. Technol. 108 (1995) 103–119.
[8] M. Tanabe, T. Bolik, C. Eigenbrod, H. Rath, J. Sato, M. Kono, Proc. Combust. Inst. 26 (1996) 1637–1643.
[9] G. Jackson, C. Avedisian, Combust. Sci. Technol. 115 (1996) 125–149.
[10] S. Cho, F. Dryer, Combust. Theory Modelling 3 (1999) 267–280.
[11] A. Marchese, F. Dryer, V. Nayagam, Combust. Flame 116 (1999) 432–459.
[12] S. Schnaubelt, O. Moriue, T. Coordes, C. Eigenbrod, H. Rath, Proc. Combust. Inst. 28 (2000) 953–960.
[13] O. Moriue, M. Mikami, K. Kojima, C. Eigenbrod, Proc. Combust. Inst. 30 (2005) 1973–1980.
[14] A. Cuoci, M. Mehl, G. Buzzi-Ferraris, T. Faravelli, D. Manca, E. Ranzi, Combust. Flame 143 (2005) 211–226.
[15] R. Stauch, S. Lipp, U. Maas, Combust. Flame 145 (2006) 533–542.
[16] J. Tsai, A. Sterling, Proc. Combust. Inst. 23 (1990) 1405–1411.
[17] A. Lee, C. Law, Combust. Sci. Technol. 86 (1992) 253–265.
[18] L.-W. Huang, C.-H. Chen, Combust. Flame 109 (1997) 145–162.
[19] J.-J. Whang, C.-Y. Yukao, J.-T. Ho, S.-C. Wong, Combust. Flame 110 (1997) 366–376.
[20] P. Stapf, H. Dwyer, R. Maly, Proc. Combust. Inst. 27 (1998) 1857–1864.

[21] J.-R. Yang, C.-Y. Yukao, J.-J. Whang, S.-C. Wong, Combust. Flame 123 (2000) 266–274.
[22] Y. Aouina, U. Maas, E. Gutheil, U. Riedel, J. Warnatz, Combust. Sci. Technol. 173 (2001) 1–23.
[23] D. Pope, G. Gogos, Numer. Heat Transfer B 48 (2005) 213–233.
[24] D. Pope, G. Gogos, Combust. Flame 142 (2005) 89–106.
[25] V. Raghavan, D. Pope, G. Gogos, J. Thermophys. Heat Transfer 20 (2006) 787–798.
[26] V. Raghavan, D. Pope, D. Howard, G. Gogos, Combust. Flame 145 (2006) 791–807.
[27] V. Raghavan, G. Gogos, V. Babu, T. Sundararajan, Int. Commun. Heat Mass Transfer 33 (2006) 686–697.
[28] G. Faeth, D. Olson, SAE Trans. (1968) 1793–1802.
[29] S. Kang, S. Baek, Combust. Sci. Technol. 164 (2001) 279–305.
[30] P. Gabele, J. Air Waste Manage. Assoc. 45 (1995) 770–777.
[31] A. Oakley, H. Zhao, N. Ladommatos, T. Ma, SAE Technical Paper 2001-01-3606, 2001.
[32] J. Hirschfelder, C. Curtiss, Proc. Combust. Inst. 3 (1949) 121–127.
[33] R. Bird, W. Steward, E. Lightfoot, Transport Phenomena, John Wiley & Sons, New York, 1960.
[34] J. Warnatz, U. Maas, R. Dibble, Combustion, third ed., Springer, Berlin, 2001.
[35] R. Reid, J. Prausnitz, B. Poling, The Properties of Gases and Liquids, fourth ed., McGraw–Hill, 1989.
[36] U. Maas, Ph.D. thesis, Universität Heidelberg, 1988.
[37] J. Hirschfelder, C. Curtiss, R. Bird, Molecular Theory of Gases and Liquids, John Wiley & Sons, New York, 1964.
[38] J. Thompson, F. Thames, C. Mastin, J. Comput. Phys. 24 (1977) 274–302.
[39] J. Steger, R. Warming, J. Comput. Phys. 40 (1981) 263–293.
[40] C. Hirsch, Numerical Computation of Internal and External Flows, vol. 2: Computational Methods for Inviscid and Viscous Flows, John Wiley & Sons, New York, 1988.
[41] U. Riedel, U. Maas, J. Warnatz, Comput. Fluids 22 (1993) 285–294.
[42] P. Deuflhard, E. Hairer, J. Zugck, Numer. Math. 51 (1987) 501–516.
[43] U. Riedel, U. Maas, J. Warnatz, Impact Comput. Sci. Eng. 5 (1993) 20–52.
[44] R. Stauch, Ph.D. thesis, Universität Karlsruhe (TH), 2007.
[45] U. Maas, J. Warnatz, Proc. Combust. Inst. 22 (1988) 1695–1704.
[46] U. Maas, J. Warnatz, Combust. Flame 74 (1988) 53–69.
[47] R. Richtmyer, K. Morton, in: I. Bers, R. Courant, J. Stoker (Eds.), Interscience Tracts in Pure and Applied Mathematics No. 4, second ed., John Wiley & Sons, 1967.
[48] W. Ranz, W. Marshall, Chem. Eng. Prog. 48 (1952) 141–146 and 173–180.
[49] W. Sirignano, Prog. Energy Combust. Sci. 9 (1983) 291–322.
[50] C. Law, Prog. Energy Combust. Sci. 8 (1982) 171–201.
[51] H. Dwyer, Prog. Energy Combust. Sci. 15 (1989) 131–158.
[52] J. Warnatz, Proc. Combust. Inst. 24 (1992) 553–579.
[53] C. Morley, GASEQ—A Chemical Equilibrium Program for Windows, http://www.gasEq.co.uk.
[54] C. Law, Combust. Flame 26 (1976) 219–233.
[55] F. Williams, Combustion Theory, second ed., Perseus, Philadelphia, 1985.
[56] W. Sirignano, Fluid Dynamics and Transport of Droplets and Sprays, Cambridge Univ. Press, Cambridge, 1999.